1   **CD4 T cells are rapidly depleted from tuberculosis granulomas following acute SIV co-**

2   **infection**

3

4   Authors: Taylor W. Foreman[1], Christine E. Nelson[1], Keith D. Kauffman[1], Nickiana E. Lora[1], Caian

5   L. Vinhaes[2,3], Danielle E. Dorosky[1], Shunsuke Sakai[1], Felipe Gomez[4], Joel D. Fleegle[4], Melanie

6   Parham[5], Shehan R. Perera[6], Cecilia S. Lindestam Arlehamn[7], Alessandro Sette[7], Tuberculosis

7   Imaging Program[4], Jason M. Brenchley[8], Artur T.L. Queiroz[2,9], Bruno B. Andrade[2,3], Juraj Kabat[10],

8   Laura E. Via [4,11,12], Daniel L. Barber[1#]

9

10   [1]T lymphocyte Biology Section, Laboratory of Parasitic Diseases, National Institutes of Allergy

11   and Infectious Disease, National Institutes of Health, Bethesda, MD, USA;

12   [2]Multinational Organization Network Sponsoring Translational and Epidemiological Research

13   (MONSTER) Initiative, Instituto Gonçalo Moniz, Fundção Oswaldo Cruz, Salvador, Brazil;

14   [3]Bahiana School of Medicine and Public Health (EBMSP), Salvador, Brazil;

15   [4]Division of Intramural Research, National Institutes of Allergy and Infectious Disease, National

16   Institutes of Health, Bethesda, MD, USA;

17   [5]Axle Informatics, National Center for Advancing Translational Sciences, Bethesda, MD, USA;

18   [6]Department of Electrical and Computer Engineering, The Ohio State University, Columbus, OH,

19   USA;

20   [7]Division of Vaccine Discovery, La Jolla Institute for Immunology, La Jolla, CA, USA;

21   [8]Barrier Immunity Section, Laboratory of Viral Diseases, National Institutes of Allergy and

22   Infectious Disease, National Institutes of Health, Bethesda, MD, USA;

23   [9]Data and Knowledge Integration Center for Health (CIDACS), Instituto Gonçalo Moniz, Salvador,

24   Bahia, Brazil;

25   [10]Biological Imaging Section, Research Technologies Branch, National Institutes of Allergy and

26   Infectious Disease, National Institutes of Health, Bethesda, MD, USA;

27   [11]Tuberculosis Research Section, Laboratory of Clinical Immunology and Microbiology, National

28   Institutes of Allergy and Infectious Disease, National Institutes of Health, Bethesda, MD, USA;

29   [12]Institute of Infectious Disease & Molecular Medicine and Division of Immunology, Department

30   of Pathology, University of Cape Town, Observatory, South Africa.

31

32   [‡]Note: The members of the NIAID/DIR Tuberculosis Imaging Program can be found at the end of

33   the Acknowledgments

34

35   [#]Corresponding author: Dr. Daniel Barber, barberd@niaid.nih.gov

36

37   Author Contributions: T.W.F. conceived and led the study. T.W.F. and D.L.B. designed the

38   research. T.W.F., C.E.N., K.D.K., N.E.L., D.E.D, and S.S. performed the experiments. T.W.F.,

39   C.E.N., A.T.L.Q., C.L., B.B.A., and D.L.B. analyzed the Luminex results. T.W.F., C.E.N., and

40   D.L.B. analyzed the flow cytometry results. T.W.F., J.K., and D.L.B. analyzed the 4D imaging

41   results. M.P. and S.R.P. wrote scripts necessary for 4D imaging analysis. C.S.L.A., A.S., and

42   J.M.B. provided critical reagents. Tuberculosis Imaging Program (TBIP) managed logistics,

43   performed NHP manipulations including infection, necropsy, PET/CT scanning, and imaging

44   analysis. F.G. and J.D.F. analysized the PET/CT data. L.E.V. supervised TBIP and designed the

45   analysis for PET/CT data. T.W.F. and D.L.B. wrote the manuscript with all authors contributing

46   with feedback.

47

2

67 **ABSTRACT**

68 The HIV-mediated decline in circulating CD4 T cells correlates with increased the risk of active

69 tuberculosis (TB)[1-4]. However, HIV/*Mycobacterium tuberculosis* (Mtb) co-infected individuals also

70 have an increased incidence of TB prior to loss of CD4 T cells in blood[3,5], raising the possibility

71 that HIV co-infection leads to disruption of CD4 T cell responses at the site of lung infection

72 before they are observed systemically. Here we used a rhesus macaque model of SIV/Mtb co-

73 infection to study the early effects of acute SIV infection on CD4 T cells in pulmonary Mtb

74 granulomas. Two weeks after SIV co-infection CD4 T cells were dramatically depleted from

75 granulomas, before significant bacterial outgrowth, disease reactivation as measured by PET-

76 CT imaging, or CD4 T cell loss in blood, airways, and lymph nodes. Mtb-specific CD4 T cells,

77 CCR5-expressing, in granulomas were preferentially depleted by SIV infection. Moreover, CD4

78 T cells were preferentially depleted from the granuloma core and lymphocyte cuff relative to B

79 cell-rich regions, and live imaging of granuloma explants showed that SIV co-infection reduced

80 T cell motility. Thus, Mtb-specific CD4 T cells in pulmonary granulomas may be decimated before

81 many patients even experience the first symptoms of acute HIV infection.

82   **MAIN**

83   Human immunodeficiency virus (HIV) infection gradually depletes circulating CD4 T cells

84   leading to the development of acquired immunodeficiency syndrome (AIDS) and impaired host

85   resistance to microbial infections. CD4 T cells are essential for control of *Mycobacterium*

86   *tuberculosis* (Mtb) infection, and tuberculosis (TB) is the leading cause of death in persons living

87   with HIV (PLWH)[6]. The extent of peripheral CD4 T cell depletion in PLWH correlates with

88   increasing risk of developing active TB[3,4]. However, PLWH with normal-to-high CD4 T cell counts

89   in the blood also have increased incidence of active TB[3]. The mechanistic basis for the elevated

90   risk of TB in individuals with normal CD4 T cell counts is incompletely understood, but may

91   reflect detrimental impact of antiviral inflammation (e.g. type I interferons) on anti-mycobacterial

92   innate immunity[7-9], impairment of macrophage function[10,11], or preferential depletion of CD4 T

93   cells in tissues compared to circulation[12-14].

94   Mtb persists in granulomas, complex structures comprised of multiple immune cell types

95   that reproducibly position themselves relative to one another[15]. Although variable by many

96   respects, granulomas can be generally described by a few key features including: an oft-

97   necrotic, macrophage-rich, core where mycobacteria are primarily located[16], a lymphocyte-rich

98   cuff circumscribing the macrophage core[17], and B cell-rich tertiary lymphoid-like substructures

99   referred to as Granuloma-Associated Lymphoid Tissue (GrALT) located within the lymphocyte

100 cuff or found as proximal granuloma satellites[18,19]. CD4 T cells are primarily found in the

101 lymphocyte cuff but can also be seen interacting with macrophages in the core or with B cells in

102 GrALT[17]. Due to the difficulty of studying human lung infections, little is understood about the

103 effects of HIV infection on Mtb granulomas. Previous studies have shown that SIV infection of

104 macaques recapitulates the gradual loss of circulating CD4 T cells and eventual development of

105 active tuberculosis disease as seen in humans[20-23]. Here we examine the very early effects of SIV

106 infection on CD4 T cell responses at the site of Mtb infection in rhesus macaques to ask if CD4

107   T cells within the granuloma microenvironment are differentially susceptible to dysfunction and

108   depletion during SIV infection as compared to T cells in circulation or lymphoid tissues.

RESULTS

To study the early effects of SIV co-infection in Mtb-infection, 10 Indian rhesus macaques were intrabronchially infected with ~56 CFU of *Mtb* H37Rv bilaterally (Fig. 1a). Animals were monitored for signs of disease for 10-11 weeks before allocation into groups that either remained Mtb *mono*-infected (n=5) or were intravenously infected with 3,000 $TCID_{50}$ of SIVmac239 (n=5). The study was concluded exactly fourteen days after SIV infection. Animals did not show signs of tuberculosis disease as measured by weight loss or fever over the course of the study (Fig. S1a-b). Plasma SIV viral loads increased in most animals until day 14 (Fig. 1b). Using RNAscope to study SIV localization, viral RNA was detected in granulomas, surrounding lung tissue, and lymph nodes (Fig. 1c-d). (Fig. 1d, S2). Spot density of RNAScope for SIV RNA was higher in granulomas than lymph node and surrounding lung tissues (Fig. 1e). Spots of viral RNA staining in granulomas were further analyzed for their distribution in the core, cuff, or GrALT (confirmed as CD20-rich areas). Viral RNA staining was most dense in GrALT regions as compared to the core and cuff of the granuloma (Fig. 1f). Although it is difficult to distinguish between viral particles and infected cells with this technique, we did find that the size of individual spots was significantly different between tissues. Lymph nodes contained a higher frequency of large spots >100 μm^2 (possibly representing infected cells) compared to the granulomas (Fig. 1g). Overall, these results demonstrate that granulomas become heavily infected with virus quickly after SIV infection.

To determine if SIV co-infection led to changes in TB lesions, macaques were imaged using ^{18}FDG PET-CT scanning prior to and 12 days after SIV co-infection (Fig. 1h). There were no changes in the number of lesions that could be identified by PET-CT imaging after SIV infection, however at necropsy, more granulomas were isolated from co-infected macaques (Fig. S1c). We found no impact of SIV infection on granuloma volumes as measured by volume of abnormal voxels or density range (Fig. 1i) or glycolytic activity as measured by ^{18}F-FDG uptake

134   (Fig. 1j). Although statistically significant, the difference in the size of granulomas was not

135   notable, and while there was a trend for increased cellularity of the SIV granulomas in co-infected

136   animals, the difference did not reach statistical significance (Fig. S1d-e). Mycobacterial loads in

137   individual granulomas were statistically significantly increased in the co-infected animals, but the

138   difference was less than 2 fold (~625 CFU in SIV-uninfected granulomas vs. ~955 CFU in co-

139   infected granulomas) (Fig. 1k). Lastly, there was no significant correlation between SIV viral and

140   mycobacterial loads in granulomas, indicating that the granulomas with lower viral loads were

141   not different due to their mycobacterial burdens (Fig. 1k). Thus, as expected we did not observe

142   tuberculosis disease reactivation in the first two weeks after SIV infection, however it is possible

143   that bacterial loads were just beginning to increase and new granulomas to form.

144   Next, we examined the effect of acute SIV infection on the pattern of soluble markers of

145   inflammation in granulomas. The markers that correlated with bacterial loads were different in

146   mono- vs co-infected granulomas (Fig. 2a). Concentrations of CCL2, CCL4, IL-8, and IL-1RA

147   were positively correlated with mycobacterial burden in the granulomas of both groups of

148   animals. In contrast, IL-6 and IL-1β levels only correlated with CFU in mono-infected granulomas,

149   and CCL3, TNF, CXCL12 and GM-CSF correlated with CFU only in the SIV co-infected

150   granulomas (Fig 2a). SIV loads in granulomas were most strongly correlated with CXCL11 (an

151   IFN-inducible CXCR3 ligand) and to a lesser extent with CCL3 and CCL4 (both CCR5 ligands)

152   as well as TNF, IL-18, and IL-23 (Fig 2a). SIV-infected granulomas contained higher levels of

153   CCL3 and IL-8, but the differences were less than ~2 fold, and the granulomas from SIV infected

154   and co-infected animals contained very similar levels of the soluble mediators measured here

155   (Fig. 2b). Thus, although SIV infection did not dramatically impact the overall levels of soluble

156   mediators in the first 2 weeks after infection, it altered the relationship between mycobacterial

157   loads and inflammatory mediators in granulomas.

158   To further characterize the impact of early SIV infection on the inflammatory milieu of

159   granulomas, we next used network density analysis of Spearman correlations[24,25] to quantify the

160   interconnectivity of these variables (Fig. 2c). After SIV infection multiple soluble mediators, in

161   particular several chemokines, had increased numbers of correlations with each other, and the

162   overall network density was significantly higher in co-infected granulomas (Fig. 2d). Most

163   notably, CXCL12 had no significant correlations with other mediators in the mono-infected

164   granulomas but was the largest node in the co-infected granulomas. Comparing the degrees of

165   connection from the bootstrap analysis highlighted the increased connectivity of CCL3, CCL4,

166   and CXCL12 in co-infected granulomas while IL-1β showed increased connectivity in mono-

167   infected granulomas (Fig. 2e). Such increased network density has previously been shown to

168   reflect heightened inflammatory states[25-27]. Interestingly, IFNα was not detected in the

169   granulomas from either group of animals, so we are unable to implicate virus-induced type IFN

170   response in these changes in the granuloma inflammatory milieu after SIV infection (Fig 2f). When

171   taken together with the overall lack of major increases in the total concentrations of most

172   mediators, and the very small increase in bacterial loads, we speculate these data indicate that

173   at 14 days after viral infection, SIV may be just beginning to drive increased mycobacterial loads

174   and perturb inflammatory responses.

175   We next examined T cell composition after co-infection. The frequency of CD4 T cells

176   was not significantly different across peripheral blood mononuclear cells (PBMCs), pulmonary

177   lymph nodes (LN), splenocytes, and bronchoalveolar lavage (BAL). In contrast, CD4 T cells were

178   greatly reduced in SIV co-infected granulomas on day 14 after SIV infection (Fig. 3a, gating

179   strategy Fig S3). Accordingly, there was no difference in the frequency of CD8 T cells in the BAL,

180   LN or spleen, but an increase was observed in granulomas from co-infected animals (Fig. S3d).

181   The difference in the CD4:CD8 T cell ratio was different between *Mtb mono*-infected and *Mtb*/SIV

182   *co*-infected granulomas (*p<0.0001*), and the decline in the CD4:CD8 cell ratio was correlated

183   with SIV viral burden (Fig. 3b). Absolute numbers of CD4 T cells were significantly reduced in co-

184   infected compared to mono-infected granulomas, while CD8 T cell numbers were retained (Fig.

185   3c). 60.5% of co-infected granulomas contained less than 20 CD4 T cells and were therefore

186   excluded from further phenotypic analysis. MTB300 peptide-specific CD4 T cells were

187   maintained in the pulmonary LN and BAL after SIV co-infection but were strikingly reduced in

188   granulomas, where the majority of granulomas no longer contained any Mtb-specific CD4 T cells

189   (Fig. 3d-e, S3e). The Mtb peptide pool used in this study is not optimized for restimulation of

190   CD8 T cells, however, Ag-specific CD8 T cells could still be detected and were not different in

191   any tissue sites of the mono and co-infected animals (Fig. S3f-g). Taken together these results

192   demonstrate that CD4 T cells, and particularly Mtb-specific CD4 T cells, are depleted from the

193   granulomas prior to detectable depletion in the peripheral tissues or even BAL, and the decline

194   in CD4 T cells is correlated with the viral burden of individual granulomas.

195   CD4 T cells are variably susceptible to SIV-mediated depletion based on activation and

196   differentiation state and expression viral entry co-receptors (e.g. CCR5)[14,28]. To examine the

197   differential susceptibility of granuloma CD4 T cell subsets to SIV co-infection, we analyzed T

198   cells for the expression of chemokine receptors CCR5, CCR6, CXCR3, CXCR5, and the

199   transcription factor eomesodermin (eomes) (Fig. S4a). We focused on the bulk population of non-

200   naïve (CD95$^+$) CD4 T cells, due to the near complete absence of Mtb-specific CD4 T cells in most

201   of the co-infected granulomas. There was a significant reduction in CCR5, CCR6, and CXCR3-

202   expressing cells, no difference in eomes$^+$ cells, and a slight increase in CXCR5$^+$ CD4 T cells in

203   co-infected compared to mono-infected granulomas (Fig. 4a-b). In contrast, among CD8 T cells

204   there was an increase in CCR5$^+$ and eomes$^+$ cell in co-infected granulomas (Fig. 4c). Consistent

205   with the granulomas, similar differences were also seen for both activated CD4 and CD8 T cells

206   in the pulmonary LN (Fig. S4b-c). Boolean gating of these markers allowed us to discriminate

207   between several relevant T cell subsets: CXCR3$^+$CCR6$^-$ Th1 cells, CCR6$^+$CXCR3$^+$ T$_H$1* cells,

208   CCR6$^+$CXCR3$^-$ Th17-like and CXCR5$^+$ Tfh-like cells (Fig. S4a). We were able to further subdivide

209   each of these subsets based on expression of the viral entry co-receptor CCR5, as well as

210   eomes. This accounted for >90% of all memory T cells in the granulomas (Fig. S4d-e). Among

211   both Th1* and Th1 cells, we found that the CCR5$^+$eomes$^-$ subset of these effector lineages was

212   preferentially depleted (Fig. 4d). In contrast, both CCR5$^+$eomes$^+$ Th1 and Th1* cells did not

213   display evidence of preferential depletion. In CD8 T cells, there was a significant increase in the

214   frequency   of   CCR5$^+$CXCR3$^+$eomes$^+$ T   cells   and   commensurate   reduction   in

215   CCR5$^+$CXCR3$^+$eomes$^-$ and CCR5$^-$CXCR3$^+$eomes$^-$ T cells from co-infected granulomas (Fig. 4e).

216   Interestingly, the increase in CCR5$^+$ CD8 T cells is consistent with the elevated levels of CCL3

217   we observed in granulomas. Thus, while the overall population of CD4 T cells in granulomas is

218   greatly reduced, there is evidence of preferential depletion of the subsets of Th1 and Th1* CD4

219   T cells that express CCR5 but lack eomes. Future experiments are needed to explore the role of

220   eomes in determining the susceptibility of CCR5$^+$ CD4 T cells to SIV-mediated depletion.

221   To determine the early effects of SIV infection on granuloma architecture and intralesional

222   T cell trafficking, we performed live-imaging of granuloma thick-section explants[24]. Live sections

223   of granulomas were stained with antibodies to CD4, CD20, and CD11b and imaged at 37°C for

224   1-2 hours (Fig 5a, Supplemental movie). Quality control was performed to remove tracks with

225   less than 5 spots or whose movement was restricted by edges in the X, Y, and Z planes (Fig.

226   S5). The X- and Y-start position of the tracks analyzed from the granuloma shown in (Fig. 5a)

227   can be seen for CD4$^+$ tracks and CD20$^+$ tracks (Fig. 5b). As expected, the number of tracks

228   normalized to the volume of tissue imaged in each granuloma was significantly lower for CD4$^+$

229   tracks in co-infected compared to mono-infected granulomas, but there was no difference in

230   CD20$^+$ tracks between the groups (Fig. 5c). Accordingly, the ratio between CD4$^+$ and CD20$^+$

231   tracks was statistically significantly reduced in granulomas imaged from co-infected macaques

232   (Fig. S6a). We next quantified the localization of tracks within the macrophage-rich core,

233   lymphocyte-rich cuff, or B cell-rich GrALT regions of granulomas (Fig. 5b). In SIV co-infected

234   granulomas, the frequency of CD4$^+$ tracks localized to GrALT was increased due to a reduction

235   in the absolute number of tracks found in the core and cuff (Fig. 5d-e). In contrast, the distribution

236   of CD20$^+$ tracks to different regions of the granuloma was not different between mono- and co-

237   infected granulomas (Fig. S6b-c). These results demonstrate CD4 T cells in the core and cuff

238   (i.e., CD4 T cells best positioned to interact with Mtb-infected macrophages), are preferentially

239   depleted early after SIV infection.

240   We next compared CD4 T cell and B cell movement in mono- and co-infected

241   granulomas. Individual tracks were categorized based on their mean speed and the variation in

242   speed into 3 major patterns of cellular motility: stopped cells, stuttering cells, or steadily moving

243   cells (Fig. 5f). CD4$^+$ tracks displayed reduced motility evidenced by a significant increase in

244   stopped tracks and concordant decrease in steadily moving tracks (Fig. 5g). This difference was

245   not seen in CD20$^+$ tracks where there was no difference stopped, steady, or stuttering tracks in

246   mono- vs co-infected granulomas (Fig. 5g). This difference was even more significant when

247   pairing the analysis of CD4$^+$ and CD20$^+$ tracks from the same granuloma indicating the changes

248   in motility are not granuloma specific but CD4 T cell specific (Fig. S6d). Taken together these

249   results demonstrate that SIV co-infection significantly decreased CD4 T cell movement in

250   granulomas.

DISCUSSION

CD4 T cell depletion is considered the primary mechanism by which HIV infection leads to the inability to control growth of Mtb, but little is understood about the impact of HIV infection on CD4 T cells at the sites of mycobacterial infection in the tissues. Here we used a non-human primate model of TB and SIV co-infection to study the early events of SIV infection on CD4 T cells in Mtb granulomas. We find that CD4 T cells in granulomas are highly sensitive to SIV-mediated depletion compared to other tissues. It is not clear why granuloma CD4 T cells are so susceptible to SIV-mediated depletion. However, it is reminiscent of the massive loss of CD4 T cells in the gastrointestinal tract of PLWH and of non-human primate species that develop AIDS after SIV infection[28-31]. Moreover, lung parenchymal CD4 T cells are more susceptible than BAL CD4 T cells to HIV mediated depletion in a humanized mouse model of HIV infection[32]. The selective loss of granuloma CD4 T cells may be due to enhanced permissiveness of these T cells to SIV infection as compared to CD4 T cells in other locations (e.g. CCR5-expressing T cells are enriched in granulomas)[33]. It is also possible that the microenvironment the granuloma itself may facilitate depletion of CD4 T cells. For example, activated macrophages efficiently take up infected CD4 T cells[34], and granulomas are densely packed with macrophages. Importantly, these two possibilities are not mutually exclusive.

In some granulomas, there was a near total loss of CD4 T cells within 14 days, indicating that most or maybe all T cells in granulomas are susceptible to depletion during SIV co-infection. Nonetheless, our data also indicate that some CD4 T cells in granulomas are even more susceptible than others. Previous reports have shown that in persons latently infected with Mtb HIV co-infection preferentially infects and depletes Mtb-specific CD4 T cells[14,35-38]. Perhaps most importantly, our data show that Mtb-specific CD4 T cells were greatly reduced in frequency in SIV co-infected granulomas long before depletion manifested in blood. CCR5-expressing Th1 and Th1* cells were also reduced in frequency in SIV co-infected granulomas. This is expected

13

276   as CCR5 is a co-receptor for viral entry. Interestingly, we found that CCR5^{+} cells that also

277   expressed the transcription factor eomes were not reduced in frequency in co-infected lesions.

278   The mechanisms underlying this apparent differential sensitivity of CCR5^{+}eomes[+] CD4 T cells is

279   not clear. Expression of CCR5 ligands in CD4 T cells has been shown previously to be associated

280   decreased viral replication in viremic patients and elite controllers[39,40], and eomes[+] CD4 T cells

281   have been shown to produce high levels of CCL3/MIP-1α[41], which may partly explain the

282   increase of soluble CCL3 in granulomas. Therefore, the preservation of CCR5^{+}eomes[+] CD4 T

283   cells in granulomas may reflect protection by CCR5-ligand production.

284   We observed a regionalized depletion where CD4 T cells were lost to a lesser degree in

285   GrALT as compared to the core and cuff of the granuloma. This was not due to a lack of viral

286   replication, as the highest amounts of virus in the granuloma as detected by RNAscope was in

287   GrALT structures. Germinal centers have been proposed to be an 'immunologically privileged'

288   site for viral persistence, perhaps due to the inability of cytotoxic T cells to interact with infected

289   T$_{FH}$ CD4 T cells, so it is possible that less effective killing by SIV-specific cytotoxic T cells may

290   be responsible for the decreased depletion of GrALT-resident CD4 T cells[42,43].

291   We also found that the CD4 T cells remaining in SIV co-infected granulomas

292   demonstrated reduced motility, raising the possibility that SIV-mediated suppression of CD4 T

293   cell movement is another mechanism of immunosuppression. HIV infection has been shown to

294   result in reduced motility of CD4 T cells in response to chemokines in vitro[44,45]. We should

295   additionally point out, however, that CD4 T cells in granulomas may also stop moving as a result

296   of interaction with peptide-presenting cells[46], so the importance of this observation to the loss

297   of bacterial control is not clear. Nonetheless, CD4 T cell interaction with infected macrophages

298   is necessary for control of intracellular mycobacterial growth[47,48], and it is possible that reduced

299   trafficking of the few remaining CD4 T cells in the granulomas further impairs microbial immunity.

300   We do not know if this defect in T cell motility occurs in other tissues, as we have only imaged

301 lung granulomas for this work. Future studies are needed to address the broader possibility that

302 lentiviral infection results in immunosuppression not only by killing T cells but also by limiting the

303 mobility the ones that remain.

304 Collectively, these data show how SIV infection is even more detrimental for Mtb-specific

305 immunity than previous appreciated. We should point out that we do not exclude other

306 mechanisms of viral infection-enhanced susceptibility to Mtb infection. Indeed, cytomegalovirus

307 infection in humans has been associated with enhanced risk of TB[49,50] and influenza infection in

308 mice has been shown to enhance Mtb infection[51]. SIV preferentially kills Mtb-specific CD4 T cells

309 in granulomas, CD4 T cells phenotypically most correlated with immune control, and CD4 T cells

310 in the subregions of granulomas that are best positioned to interact with Mtb-infected

311 macrophages. To make things worse, it impairs the trafficking of the CD4 T cells that remain.

312 Most patients are just beginning to notice signs and symptoms of HIV infection 14 days after

313 primary infection, yet here we demonstrate that CD4 T cells within the granuloma have already

314 been depleted. These data provide a potential explanation of the increased risk of TB reactivation

315 prior to the loss of peripheral CD4 T cells in HIV infection. Understanding the granuloma-specific

316 mechanisms CD4 T cell susceptibility to SIV-mediated depletion may lead to intervention

317 strategies to preserve anti-tuberculosis immunity in co-infected individuals.

318 **METHODS**

319 Study Design and Infections

320   Rhesus macaques originally from the Morgan Island NIH breeding colony were housed

321 in biocontainment according to the Animal Welfare Act and the Guide for the Care and Use of

322 Laboratory Animals within a AAALAC international-accredited animal biosafety level-3 vivarium.

323 Daily enrichment was provided for the macaques. All procedures were performed using

324 anesthetics according to the approved NIAID DIR Animal Care and Use Committee study

325 proposal LPD-25E. Additionally, animals were scanned at regular intervals with a LFER 150

326 PT/CT scanner (Mediso, Inc., Hungary) using ^{18}FDG (0.5 mCi/kg) and tubercular lung disease, as

327 well as, individual lesion characteriztics were analyzed on serial scans as described

328 previously[24,52]. The object of this study was to understand the effects of acute SIV on Mtb-

329 specific immune responses. To achieve this, 10 macaques were intrabronchially infected with

330 ~56 CFU of *Mycobacterium tuberculosis* (*Mtb*) strain H37Rv-mCardinal (kindly provided by Dr.

331 Clifton Barry III, chief of the Tuberculosis Research Section, Laboratory of Clinical Immunology

332 and Microbiology, NIAID) bilaterally using 2-mL of saline each into the right and left lower lobes

333 (14.0 ± 3.77 CFU/mL). After *Mtb* infection, animals were montored for clinical signs of

334 tuberculosis such as weight loss and pyrexia for 10-11 weeks. Thereafter animals were randomly

335 assigned to one of two groups where the *mono*-infection group remained SIV-naïve and the co-

336 infection group was intravenously injected with 3,000 $TCID_{50}$ of SIVmac239. For tissue collection

337 exactly 14 days post SIV infectioin, a co-infection animal along with a time-matched *Mtb* mono-

338 infected animal was euthanized according to American Veterinary Medical Association

339 guidelines.

340

341 Tissue Processing for Cells, Bacteria, and Virus

16

342 Blood was collected using EDTA-tubes and cells isolated using Ficoll-Paque Density

343 Centrifugation (GE Life Sciences, Canada). Bronchoalveolar lavage (BAL) was collected using a

344 modified feeding tube inserted through the trachea into the lower pulmonary lobes and lavaged

345 using ~60mL of sterile saline. Fluid was then filtered using a 100-micron filter and centrifuged for

346 the collection of cells. Tissues were taken for analysis at the time of necropsy. For single cell

347 suspensions, spleen and lymphnodes were homogenized using gentleMACSs dissociators

348 (Miltenyi Biotec, Germany) and filtered through a 100-micron filter while isolated granulomas

349 were mashed through a 100-micron filter using a syringe plunger. Homogenates from

350 granulomas and tissues were serially diluted and plated on 7H11 agar plates incubated at 37°C

351 for 3-4 weeks before quantification. Granuloma homogenate was taken for RNA isolation using

352 RNeasy Plus Kits and stored at -80°C (Qiagen, USA). Quantification of viral burden was done

353 using TaqPath 1-step RT-qPCR Master Mix (Thermo Fisher Scientific, USA) and primers/probes

354 sets targeting SIVmac239 (Eurofins Scientific, USA) or GAPDH (Thermo Fisher Scientific, USA).

355 Reactions were completed in triplicates for 40 cycles using FAM dyes. Plasma was filter-

356 sterilized and analyzed for plasma viral load by RT-qPCR by Quantitative Molecular Diagnostics

357 Core at the Frederick National Laboratory.

358

359 Cell stimulation and Flow cytometry

360 Cells were stimulated with 2 μg/mL of MTB300 epitope peptide pool (A&A Labs, USA) in

361 the presence of brefeldin A and monensin (Thermo Fisher Scientific, USA) for 6 hours at 37°C in

362 Complete media (RPMI-1640 with 10% fetal calf serum (FCS), 1% Sodium pyruvate, 1%

363 penicillin and streptomycin, 25 mM Hepes, and 2 mM l-glutamate). Fresh cells were incubated

364 in blocking buffer containing 1% FCS, 1μg/mL Human FC block (BD Biosciences, USA) for 1-6

365 hours at 4°C. Cells were then stained using fixable live/dead stain for 20 minutes at room

366 temperature. Surface antibody staining was done in PBS containing 1% FCS and 1X Brilliant

17

367   Stain Buffer (BD Biosciences, USA) for 20 minutes at room temperature. After fixation and

368   permeabilization using Foxp3/Transcription Factor Staining Kit (eBiosciences, USA), intracellular

369   antibody staining was done in PBS containing 1% FCS, 1X Brilliant Stain Buffer, and 1X

370   Permeabilization reagent for 30 minutes at 4°C. Samples were acquired using a FACSymphony

371   cytometer (BD Biosciences, USA) and data analyzed using FlowJo 10 (BD Biosciences, USA).

372   Gating strategies are shown in figures S3-4.

373

374   Multiplex cytokine analysis

375   Granuloma homogenates were filter-sterilized and processed for soluble protein marker

376   concentrations using the Invitrogen Cytokine and Chemokine 30-Plex ProcartaPlex Kit (Thermo

377   Fisher Scientific, USA) according to manufacturer protocol. Samples were acquired using a

378   MAGPIX with xPONENT software (Luminex Corporation, USA). Soluble marker protein levels

379   were normalized to total protein levels measured by Quant-iT protein Assay Kit (Thermo Fisher

380   Scientific, USA).

381

382   4D Confocal Imaging of Granulomas

383   Isolated granulomas were kept on ice until embedding in PBS with 2% agarose. The

384   tissue was cut into 300-micron thick sections using a Leica VT1000 S Vibrating Blade Microtome

385   (Leica Microsystems, USA) housed in Class II, Biosafety hood within a BSL3 laboratory. Sections

386   of tissue were incubated in 1X PBS supplemented with 10% FCS, isotype-specific blocking

387   antibodies, and Human FC Block (BD Biosciences, USA) for 2-8 hours at 4°C. After blocking,

388   tissues were stained with antibodies CD4, CD20, and CD11b for 2-12 hours at 4°C with

389   intermittent shaking. Tissues were then washed and placed into chamber slides containing

390   Complete Imaging Media (Complete media made with phenol red-free RPMI) supplemented with

391   ProLong Live Antifade Reagent (Thermo Fisher Scientific, USA). After incubation in a 5% CO_2

392   incubation chamber at 37°C for 1 hour, the chambered slide was imaged using Leica SP5

393   inverted confocal microscope with environmental chamber to maintain the sample humidified at

394   37°C (Leica Microsystems, USA). Sections were serially imaged over the course of 1-2 hours

395   and compiled using LAS X software (Leica Microsystems, USA). Image analysis was performed

396   using Imaris software (Bitplane, Switzerland) for quantification of individual cells using the spot

397   function to track their movement over time. Data from tracks were exported, processed through

398   a custom Python 3 script to select the parameters to include in the exported files, and then

399   imported into FlowJo 10 software (BD Biosciences, USA) for data visualization and analysis as

400   described in Fig S6. Briefly, tracks that were limited in movement by the edges of the X-, Y-, or

401   Z-plane were excluded from analysis. Using the X- and Y-starting point of a track, cells could be

402   localized to different areas in the granuloma. Finally, track movement was categorized into three

403   different forms. Stopped and Steady tracks both had ≤0.90 μm/minute track speed variation but

404   were characterized by ≤2.0 μm/minute or >2.0 μm/minute mean track speed, respectively.

405   Stuttering tracks had any mean track speed but were characterized by track speed variation

406   >0.90 μm/minute.

407

408   RNAscope and Image Analysis

409   Formalin Fixed Paraffin embedded tissues sections were cut into 10-micron thick

410   sections using RNAse precautions and used for RNAscope *in situ* hybridization staining for viral

411   RNA (ACD Biotechne, USA). Slides were dewaxed using xylene and ethanol and then underwent

412   epitope retrieval using heat induced low-pH methods according to the manufacturer. Slides were

413   then treated with diluted protease plus for 20 min at 40°C and endogenous peroxidases blocked

414   using hydrogen peroxide for 10 min at room temperature. Probes for SIVmac239, containing 83

415   separate pairs of probes spanning the proviral gag, vif, pol, tat, env, vpx, vpr, nef, and rev genes,

416   were used for single color immunohistochemistry with hematoxylin counter-staining using the

417 RNAscope 2.5 HD Assay-RED (ACD Biotechne, USA). Immunocytochemically stained slides

418 were imaged using Aperio VERSA (Leica Microsystems, USA) and analyzed using a custom

419 quPath script to identify spots with pixel size 0.5-microns, background radius 8-microns, median

420 radius 8-microns, sigma 0.75-microns, minimum area 2.0-microns, maximum area 400-microns,

421 with threshold of 0.25. Spots were then colocalized to granuloma regions using annotation tabs

422 for each area of the granuloma which were identified according to the different hematoxylin

423 counter-staining pattern and CD20 staining.

424

425 Statistical analyses

426 All statistical analyses were conducted using GraphPad Prism V8 (GraphPad Software,

427 USA) except for when specified otherwise. Data were tested for Gaussian distribution using the

428 DÁgostino's K-square test. For group comparisons, individual tests vary and are denoted in each

429 figure legend but include two-tailed unpaired T-tests, Mann-Whitney *U* (when parameter

430 compared were not normally distributed), One-way ANOVA with correction for multiple tests

431 using Tukey Multiple Comparison test corrections, non-linear regression analysis of semi-log

432 line, or simple linear regression analysis. Multiplex Luminex assay data were analyzed using R

433 4.0.2 packages *igraph*, *ggplot2*, *viridis*, *ComplexHeatmap*, *Hmisc*, with *p.adjust* function. Fold

434 change was measured and significance test by Student's T test with False Discovery Ratio

435 correction. Correlation analyses were performed using the Spearman's rank test with 100

436 bootstrap replicates. Bootstrap threshold value was defined in 80 replicates. Significant values

437 were corrected using False Discovery Ratio. Any place p-value are reported in asterisks * $p < 0.05$,

438 ** $p < 0.01$, *** $p < 0.001$, and **** $p < 0.0001$, ns=non-signficant.

Figure legends

Figure 1. Lung Mtb granulomas are heavily infected by SIV rapidly after co-infection. (A) 10 Rhesus macaques were intrabronchially infected with Mycobacterium tuberculosis H37Rv for 10-11 weeks and 5 macaques were subsequently infected with SIVmac239 intravenously. Both groups were followed for another 14 days. (B) Acute viral infection was tracked by measuring plasma viral loads after co-infection. (C) Example image of RNAscope staining for SIV viral RNA in a co-infected granuloma. (vRNA shown in red and nuclei counterstained light blue) (D) Quantification of individual spots was performed and compared to different microanatomical locations in the granuloma as indicated and verified by immunohistochemical staining for B cell clusters. (E) Quantification of the number of SIV spots analyzed in uninvolved lung tissue and lymph nodes compared to granulomas. (F) Different regions of the granuloma were further characterized demonstrating increased viral burden in GrALT. (G) Distribution violin plots of the size in μm^2 of individual spots with the frequency of >100 μm spots indicated above the boxed area. (H) ^{18}FDG PET-CT scans were performed immediately before SIV infection and at day 12 post co-infection which allowed tracking individual lesions. (I) The change in volume of each lesion as measured in voxels (0.5 mm^3) with with abnormal houndsfeld unit density (-400 to 200 HU) on CT was insiginifcant from pre- to post-SIV infection. (J) ^{18}FDG uptake, expressed as the total lesion glycolytic (TLG) activity in standardized uptake value/body weight (SUVbw)/mL, of each lesion was compared pre- to post-SIV infection and also found to be insignificant. (K) Individual granulomas were isolated at the time of necropsy for determination of bacterial load. (L) RNA isolated from each granuloma was assayed for viral quantification and compared to bacterial burden. Statistical analysis was calculated using (E-F) one-way ANOVA, (I-J) student's unpaired T-tests, (K) Mann-Whitney U-test, or (L) nonlinear regression analysis. ns = non-significant, ** p<0.01, *** p<0.001 **** p<0.0001

464 **Figure 2. Early changes in soluble mediators in Mtb granulomas after SIV co-infection.** (A)

465 Granuloma homogenates were assayed for soluble mediators of inflammation, values normalized

466 to protein levels and by Z-score and compared to bacterial and viral burdens. Heatmap

467 visualization of 23 markers within mono-infected (left) and co-infected (right) granulomas with

468 indicated bacterial burden for each granuloma shown below the heatmap, and spearman

469 correlations with pathogen burdens to the right. Correlations were calculated intra-group and

470 only values with false discovery rate below 0.01 highlighted as significant. (B) The log2 fold

471 change of soluble markers between mono- and co-infected groups were calculated and

472 compared for significance. (C) Correlation network analysis using Spearman's rank test were

473 performed and visualized using circus plots where the size of the circle indicates the number of

474 significant correlations. (D) The overall distribution of network density degree and (E) individual

475 degrees of connectivity of CCL3, CCL4, CXCL12, and IL-1β in 100 bootstrap replicates. (F) The

476 levels of IFNα in granuloma homogenates of all samples shown in correlation to viral burden.

477 Statistical analysis was performed using (A) Spearman's rank test for correlations, (B, D-E)

478 student's T test with false discovery ratio correction, or (E) Wilcoxon signed-rank test.

479

480 **Figure 3. Mtb-specific CD4 T cells are massively depleted in granulomas two weeks after**

481 **SIV co-infection.** (A) Flow cytometric analysis of PBMC's, pulmonary lymph nodes (LN),

482 splenocytes, bronchoalveolar lavage (BAL), and individual granulomas showing the percentage

483 of CD3$^+$ T cells that are CD4$^+$. (B) Comparison of the CD4:CD8 ratio in individual granulomas to

484 the viral burden. (C) Quantification of the number of total CD4$^+$ and CD8$^+$ T cells in granulomas.

485 LOD = Limit of detection. (D) Example flow cytometry plots of Mtb antigen stimulation of CD4$^+$ T

486 cells in pulmonary LN, BAL, and granulomas from mono- and co-infected (top and bottom row,

487 respectively). (E) Frequency and absolute number of antigen specific CD4$^+$ T cells in granulomas

488 after restimulation with a Mtb peptide pool. Statistical analysis was calculated using (A) students

489   unpaired T-tests, (B) nonlinear regression analysis, or (C, E) Mann-Whitney U-test. ** p<0.01, ****

490   p<0.0001

491

492   **Figure 4. CCR5-expressing Th1 and Th1* cells in granulomas are preferentially depleted**

493   **by SIV co-infection.** (A) Example flow cytometry plots of activated CD4 T cells in granulomas

494   expressing chemokine receptors CCR5, CCR6, CXCR3, CXCR5, and the transcription factor

495   eomesodermin (eomes). (B-C) Expression of markers in non-naïve CD4 T cells and CD8 T cells.

496   (D-E) Boolean analysis of the same markers where the ten populations of cells shown comprise

497   >90% of total population of CD4 and CD8 T cells. Statistical analysis was calculated using

498   Student's unpaired T-tests. * p<0.05, ** p<0.01, *** p<0.001, **** p<0.0001

499

500   **Figure 5. SIV co-infection alters the spatial distribution and intralesional trafficking of CD4**

501   **T cells in Mtb granulomas.** (A-B) Example still image of a granuloma used for 4D imaging (CD4

502   is cyan, CD20 is green, and CD11b is purple) where distilled cellular tracks from CD4$^+$ and CD20$^+$

503   cells shown in the X- and Y-start position. (C) Absolute number of tracks normalized to the

504   volume of tissue imaged. (D-E) Localization of CD4$^+$ tracks within the macrophage rich core, the

505   lymphocyte dense cuff, or the granuloma-associated lymphoid tissue that forms within the cuff

506   as the frequency of or absolute number of total CD4$^+$ tracks in the granuloma. (F) Example plots

507   of the movement of CD4$^+$ tracks from a single granuloma with frequency denoted in the top right

508   corner. (G) Quantification of the movement of CD4$^+$ tracks and CD20$^+$ tracks as denoted as

509   stopped, steadily moving, or stuttering. Statistical analysis was calculated using students

510   unpaired T-tests. * p<0.05, ** p<0.01

511

512   **Supplemental Figure 1. Clinical parameters in mono- and co-infected macaques.** (A-B)

513   Weight change as percent deviation from starting weight and rectal temperature over the course

23

514　　of the study. (C) Quantification of the number of visible lesions by PET/CT imaging at pre- and

515　　post-SIV viral infection along with the number of lesions isolated at the time of necropsy. (D) The

516　　diameter of individual granulomas measured at necropsy. (E) Number of cells isolated per

517　　granuloma after processing for single cell suspensions. Statistical analysis was calculated using

518　　(C) paired Student's T test or (D-E) Mann-Whitney U-test. ns = not significant

519

520　　**Supplemental Figure 2. RNAscope imaging quantification of SIV RNA**. (A-B) RNAscope

521　　image of a SIV-infected granuloma with SIV viral RNA shown in red with a light blue nuclei

522　　counterstain with higher-magnification image inset. (C-D) Quantification of viral spots using

523　　QuPath Image analysis, shown as yellow spots with the same high-magnification image shown

524　　above. (E) Example gating pattern for the localization of spots throughout the granuloma. (F)

525　　Image of SIV-naïve granuloma to demonstrate the high specificity of in situ hybridization.

526

527　　**Supplemental Figure 3. T cell gating strategy.** Shown is an example flow cytometric gating

528　　strategy for a single cell suspension from a pulmonary LN. (A) Parent gates for lymphocytes, live

529　　cells, and singlets with progression to $CD3^+$ T cells and frequency of $CD4^+$ to $CD8^+$ T cells.

530　　Detailed analysis of T cells starting from parent gates and progressing to (B) $CD3^+CD4^+CD8^-$

531　　$CD95^+$ T cells or (C) $CD3^+CD4^-CD8^+CD95^+$ T cells. (D) Frequency of $CD3^+$ T cells that are $CD8^+$

532　　in the blood, pulmonary LN, spleen, and BAL. (E) Frequency of Mtb-specific $CD4^+$ T cells in the

533　　pulmonary LN and BAL at the time of necropsy. (F) Example flow cytometry plots of $CD8^+$ T cells

534　　stimulated with Mtb peptide pools (14-mer epitopes) and the (G) quantification of antigen-

535　　specific $CD8^+$ T cells in granulomas, BAL, and pulmonary LN's. Statistical analysis was

536　　calculated using Student's unpaired T-tests. **** $p<0.0001$

537

538 **Supplemental Figure 4. Differential depletion of phenotypically distinct CD4 T cell subsets.**

539 (A) Example gating strategy used for the Boolean analysis of CCR5, CCR6, CXCR3, CXCR5, and

540 eomes in both CD4$^+$ and CD8$^+$ T cells. Parent gate represents gating strategy shown in

541 Supplemental Figure 3 as labelled above initiating plots. (B-C) Expression of these markers on

542 activated CD4 and CD8 T cells from the pulmonary LN. (D-E) Quantification of the percent of

543 total CD4 and CD8 T cells comprised of the 10 populations shown in Fig. 4D-E. Statistical

544 analysis was calculated using students unpaired T-tests. * $p<0.05$, **** $p<0.0001$

545

546 **Supplemental Figure 5. Analysis strategy for 4D imaging of granulomas.** (A) Example plots

547 of the stringent parameters used to isolate CD4 and CD20 tracks. Only tracks with more than or

548 equal to 5 individual spots were used, with cells excluded that were inhibited by the Z, X, or Y

549 boundaries. (B) The tracks analyzed for this granuloma with comparison of a still-image. (C) High-

550 magnification image shows spots analyzed overlayed with the actual image. (D) Example flow

551 plots of cellular movement in two different granulomas showing the range of movement and

552 indicated movement characteristics.

553

554 **Supplemental Figure 6. Analysis of cellular movement in granulomas.** (A) Ratio of CD4 to

555 CD20 tracks in all granulomas analyzed by 4D imaging. (B-C) Quantification of the frequency

556 and absolute number of CD20 tracks from the core, cuff, and GrALT. (D) Paired analysis of

557 CD4 and CD20 tracks from the same granuloma to show the reduction in movement as

558 specific to T cells and not the whole granuloma. Statistical analysis was calculated using (A-C)

559 students unpaired T-tests and (D) paired T-tests. * $p<0.05$, *** $p<0.001$, **** $p<0.0001$

560   REFERENCES
561

562   **Uncategorized References**

563   1.   Geldmacher, C., Zumla, A. & Hoelscher, M. Interaction between HIV and *Mycobacterium*
564   *tuberculosis*: HIV-1-induced CD4 T-cell depletion and the development of active
565   tuberculosis. *Curr Opin HIV AIDS* **7**, 268-275 (2012).
566   2.   Okoye, A.A. & Picker, L.J. CD4(+) T-cell depletion in HIV infection: mechanisms of
567   immunological failure. *Immunol Rev* **254**, 54-64 (2013).
568   3.   Glynn, J.R.*, et al.* Effects of duration of HIV infection and secondary tuberculosis
569   transmission on tuberculosis incidence in the South African gold mines. *AIDS* **22**, 1859-
570   1867 (2008).
571   4.   van der Sande, M.A.*, et al.* Incidence of tuberculosis and survival after its diagnosis in
572   patients infected with HIV-1 and HIV-2. *AIDS* **18**, 1933-1941 (2004).
573   5.   Esmail, H.*, et al.* The Immune Response to *Mycobacterium tuberculosis* in HIV-1-
574   Coinfected Persons. *Annu Rev Immunol* **36**, 603-638 (2018).
575   6.   *Global Tuberculosis Report 2019*, (Geneva: World Health Organization, 2019).
576   7.   Mayer-Barber, K.D.*, et al.* Host-directed therapy of tuberculosis based on interleukin-1
577   and type I interferon crosstalk. *Nature* **511**, 99-103 (2014).
578   8.   Zhang, L., Jiang, X., Pfau, D., Ling, Y. & Nathan, C.F. Type I interferon signaling mediates
579   *Mycobacterium tuberculosis*-induced macrophage death. *J Exp Med* **218**(2021).
580   9.   Sandler, N.G.*, et al.* Type I interferon responses in rhesus macaques prevent SIV infection
581   and slow disease progression. *Nature* **511**, 601-605 (2014).
582   10.   DiNapoli, S.R., Hirsch, V.M. & Brenchley, J.M. Macrophages in Progressive Human
583   Immunodeficiency Virus/Simian Immunodeficiency Virus Infections. *J Virol* **90**, 7596-7606
584   (2016).
585   11.   Kuroda, M.J.*, et al.* High Turnover of Tissue Macrophages Contributes to Tuberculosis
586   Reactivation in Simian Immunodeficiency Virus-Infected Rhesus Macaques. *J Infect Dis*
587   **217**, 1865-1874 (2018).
588   12.   Brenchley, J.M.*, et al.* CD4+ T cell depletion during all stages of HIV disease occurs
589   predominantly in the gastrointestinal tract. *J Exp Med* **200**, 749-759 (2004).
590   13.   Picker, L.J.*, et al.* Insufficient production and tissue delivery of CD4+ memory T cells in
591   rapidly progressive simian immunodeficiency virus infection. *J Exp Med* **200**, 1299-1314
592   (2004).
593   14.   Geldmacher, C.*, et al.* Preferential infection and depletion of *Mycobacterium tuberculosis*-
594   specific CD4 T cells after HIV-1 infection. *J Exp Med* **207**, 2869-2881 (2010).
595   15.   Pagan, A.J. & Ramakrishnan, L. The Formation and Function of Granulomas. *Annu Rev*
596   *Immunol* **36**, 639-665 (2018).
597   16.   Mattila, J.T.*, et al.* Microenvironments in tuberculous granulomas are delineated by
598   distinct populations of macrophage subsets and expression of nitric oxide synthase and
599   arginase isoforms. *J Immunol* **191**, 773-784 (2013).
600   17.   Kauffman, K.D.*, et al.* Defective positioning in granulomas but not lung-homing limits CD4
601   T-cell interactions with *Mycobacterium tuberculosis*-infected macrophages in rhesus
602   macaques. *Mucosal Immunol* **11**, 462-473 (2018).

603 18. Ulrichs, T.*, et al.* Human tuberculous granulomas induce peripheral lymphoid follicle-like
604   structures to orchestrate local host defence in the lung. *J Pathol* **204**, 217-228 (2004).
605 19. Phuah, J.Y., Mattila, J.T., Lin, P.L. & Flynn, J.L. Activated B cells in the granulomas of
606   nonhuman primates infected with *Mycobacterium tuberculosis*. *Am J Pathol* **181**, 508-514
607   (2012).
608 20. Foreman, T.W.*, et al.* CD4+ T-cell-independent mechanisms suppress reactivation of
609   latent tuberculosis in a macaque model of HIV coinfection. *Proc Natl Acad Sci U S A* **113**,
610   E5636-5644 (2016).
611 21. Diedrich, C.R.*, et al.* SIV and *Mycobacterium tuberculosis* synergy within the granuloma
612   accelerates the reactivation pattern of latent tuberculosis. *PLoS Pathog* **16**, e1008413
613   (2020).
614 22. Larson, E.C.*, et al.* Pre-existing Simian Immunodeficiency Virus Infection Increases
615   Expression of T Cell Markers Associated with Activation during Early *Mycobacterium*
616   *tuberculosis* Coinfection and Impairs TNF Responses in Granulomas. *J Immunol* (2021).
617 23. Ganatra, S.R.*, et al.* Antiretroviral therapy does not reduce tuberculosis reactivation in a
618   tuberculosis-HIV coinfection model. *J Clin Invest* **130**, 5171-5179 (2020).
619 24. Kauffman, K.D.*, et al.* PD-1 blockade exacerbates *Mycobacterium tuberculosis* infection in
620   rhesus macaques. *Sci Immunol* **6**(2021).
621 25. Vinhaes, C.L.*, et al.* Dissecting disease tolerance in *Plasmodium vivax* malaria using the
622   systemic degree of inflammatory perturbation. *PLoS Negl Trop Dis* **15**, e0009886 (2021).
623 26. Tiburcio, R.*, et al.* Dynamics of T-Lymphocyte Activation Related to Paradoxical
624   Tuberculosis-Associated Immune Reconstitution Inflammatory Syndrome in Persons With
625   Advanced HIV. *Front Immunol* **12**, 757843 (2021).
626 27. Bruyn, E.D.*, et al.* Inflammatory profile of patients with tuberculosis with or without HIV-
627   1 co-infection: a prospective cohort study and immunological network analysis. *Lancet*
628   *Microbe* **2**, e375-e385 (2021).
629 28. Okoye, A.*, et al.* Progressive CD4+ central memory T cell decline results in CD4+ effector
630   memory insufficiency and overt disease in chronic SIV infection. *J Exp Med* **204**, 2171-
631   2185 (2007).
632 29. Veazey, R.S.*, et al.* Identifying the target cell in primary simian immunodeficiency virus
633   (SIV) infection: highly activated memory CD4(+) T cells are rapidly eliminated in early SIV
634   infection in vivo. *J Virol* **74**, 57-64 (2000).
635 30. Mattapallil, J.J.*, et al.* Massive infection and loss of memory CD4+ T cells in multiple tissues
636   during acute SIV infection. *Nature* **434**, 1093-1097 (2005).
637 31. Brenchley, J.M.*, et al.* Differential Th17 CD4 T-cell depletion in pathogenic and
638   nonpathogenic lentiviral infections. *Blood* **112**, 2826-2835 (2008).
639 32. Corleis, B.*, et al.* HIV-1 and SIV Infection Are Associated with Early Loss of Lung Interstitial
640   CD4+ T Cells and Dissemination of Pulmonary Tuberculosis. *Cell Rep* **26**, 1409-1418 e1405
641   (2019).
642 33. Paiardini, M.*, et al.* Low levels of SIV infection in sooty mangabey central memory CD(4)(+)
643   T cells are associated with limited CCR5 expression. *Nat Med* **17**, 830-836 (2011).
644 34. Calantone, N.*, et al.* Tissue myeloid cells in SIV-infected primates acquire viral DNA
645   through phagocytosis of infected T cells. *Immunity* **41**, 493-502 (2014).

646 35. Bunjun, R.*, et al.* Th22 Cells Are a Major Contributor to the Mycobacterial CD4(+) T Cell
647   Response and Are Depleted During HIV Infection. *J Immunol* **207**, 1239-1249 (2021).
648 36. Strickland, N.*, et al.* Characterization of *Mycobacterium tuberculosis*-Specific Cells Using
649   MHC Class II Tetramers Reveals Phenotypic Differences Related to HIV Infection and
650   Tuberculosis Disease. *J Immunol* (2017).
651 37. Geldmacher, C.*, et al.* Early depletion of *Mycobacterium tuberculosis*-specific T helper 1
652   cell responses after HIV-1 infection. *J Infect Dis* **198**, 1590-1598 (2008).
653 38. Amelio, P.*, et al.* HIV Infection Functionally Impairs *Mycobacterium tuberculosis*-Specific
654   CD4 and CD8 T-Cell Responses. *J Virol* **93**(2019).
655 39. Kinter, A.L.*, et al.* HIV replication in CD4+ T cells of HIV-infected individuals is regulated by
656   a balance between the viral suppressive effects of endogenous beta-chemokines and the
657   viral inductive effects of other endogenous cytokines. *Proc Natl Acad Sci U S A* **93**, 14076-
658   14081 (1996).
659 40. Casazza, J.P.*, et al.* Autocrine production of beta-chemokines protects CMV-Specific CD4
660   T cells from HIV infection. *PLoS Pathog* **5**, e1000646 (2009).
661 41. Buggert, M.*, et al.* Limited immune surveillance in lymphoid tissue by cytolytic CD4+ T
662   cells during health and HIV disease. *PLoS Pathog* **14**, e1006973 (2018).
663 42. Mylvaganam, G.H.*, et al.* Dynamics of SIV-specific CXCR5+ CD8 T cells during chronic SIV
664   infection. *Proc Natl Acad Sci U S A* **114**, 1976-1981 (2017).
665 43. Cadena, A.M.*, et al.* Persistence of viral RNA in lymph nodes in ART-suppressed SIV/SHIV-
666   infected Rhesus Macaques. *Nat Commun* **12**, 1474 (2021).
667 44. Cecchinato, V.*, et al.* Impairment of CCR6+ and CXCR3+ Th Cell Migration in HIV-1
668   Infection Is Rescued by Modulating Actin Polymerization. *J Immunol* **198**, 184-195 (2017).
669 45. Perez-Patrigeon, S.*, et al.* HIV infection impairs CCR7-dependent T-cell chemotaxis
670   independent of CCR7 expression. *AIDS* **23**, 1197-1207 (2009).
671 46. Egen, J.G.*, et al.* Intravital imaging reveals limited antigen presentation and T cell effector
672   function in mycobacterial granulomas. *Immunity* **34**, 807-819 (2011).
673 47. Grace, P.S. & Ernst, J.D. Suboptimal Antigen Presentation Contributes to Virulence of
674   *Mycobacterium tuberculosis* In Vivo. *J Immunol* **196**, 357-364 (2016).
675 48. Yang, J.D.*, et al. Mycobacterium tuberculosis*-specific CD4+ and CD8+ T cells differ in their
676   capacity to recognize infected macrophages. *PLoS Pathog* **14**, e1007060 (2018).
677 49. Muller, J.*, et al.* Cytomegalovirus infection is a risk factor for tuberculosis disease in
678   infants. *JCI Insight* **4**(2019).
679 50. Martinez, L.*, et al.* Cytomegalovirus acquisition in infancy and the risk of tuberculosis
680   disease in childhood: a longitudinal birth cohort study in Cape Town, South Africa. *Lancet
681   Glob Health* **9**, e1740-e1749 (2021).
682 51. Redford, P.S.*, et al.* Influenza A virus impairs control of *Mycobacterium tuberculosis*
683   coinfection through a type I interferon receptor-dependent pathway. *J Infect Dis* **209**, 270-
684   274 (2014).
685 52. Beites, T.*, et al.* Plasticity of the *Mycobacterium tuberculosis* respiratory chain and its
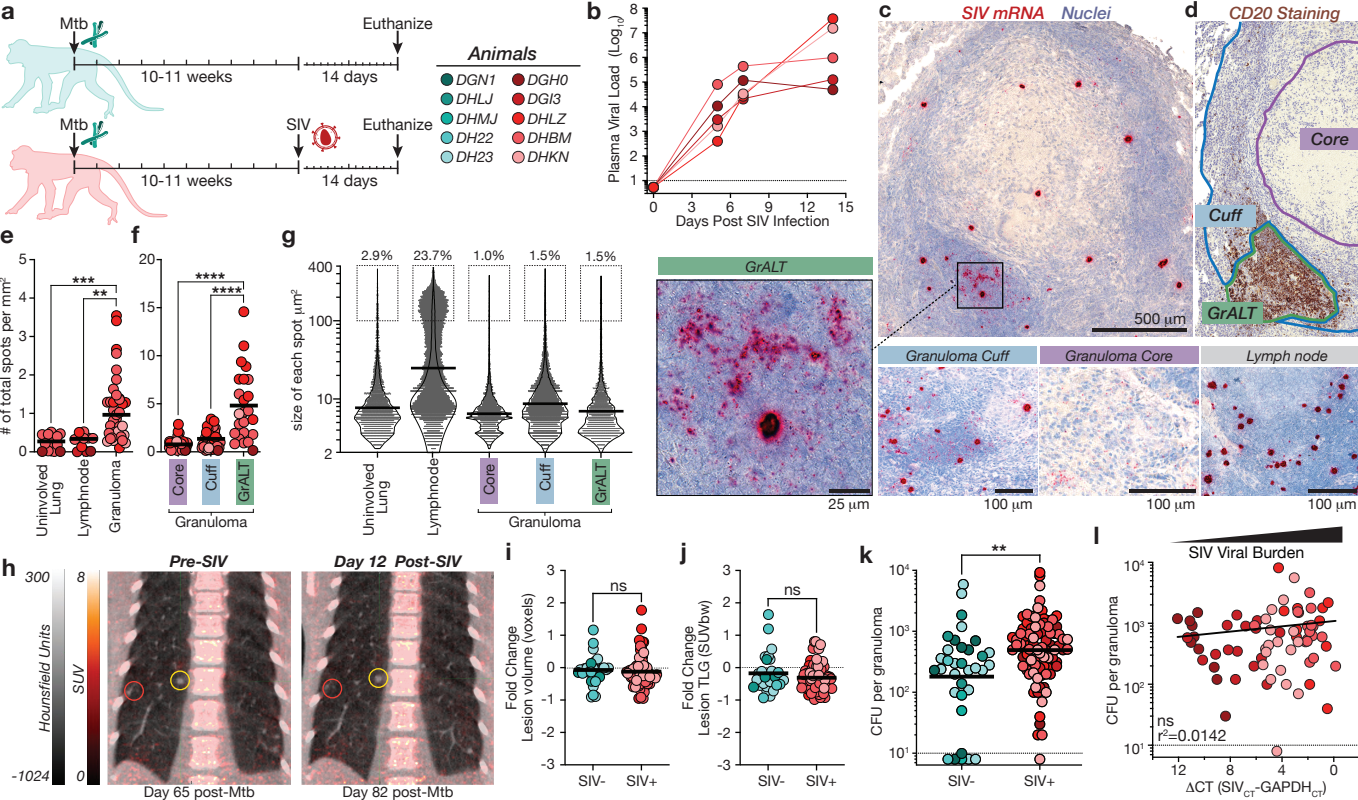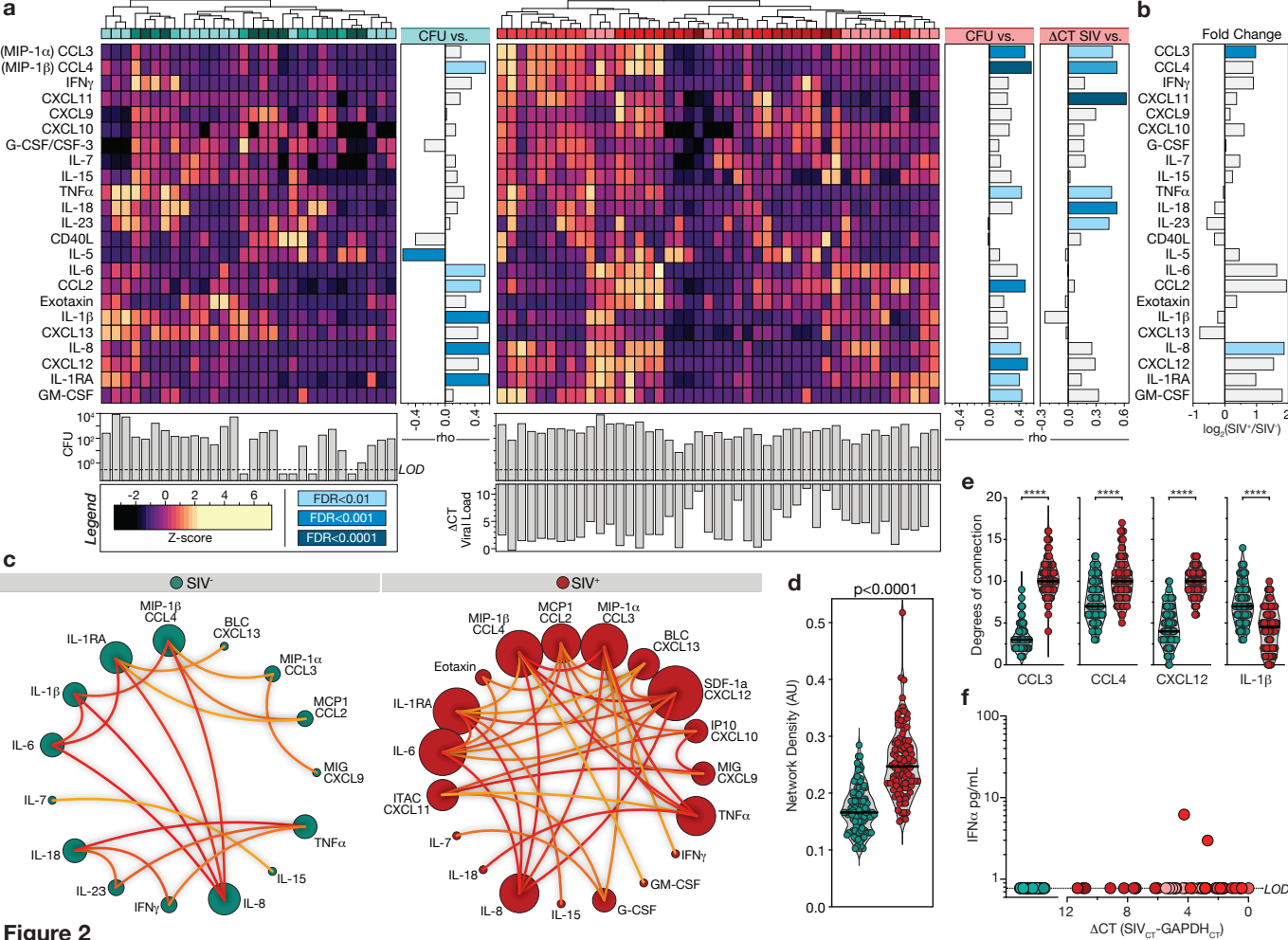686   impact on tuberculosis drug development. *Nat Commun* **10**, 4970 (2019).
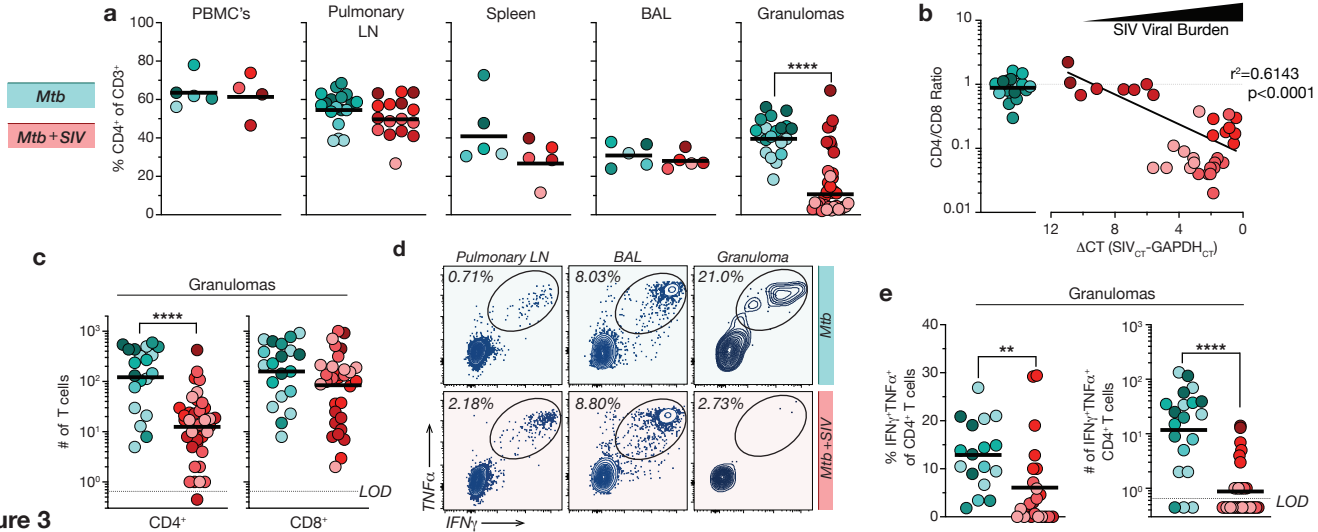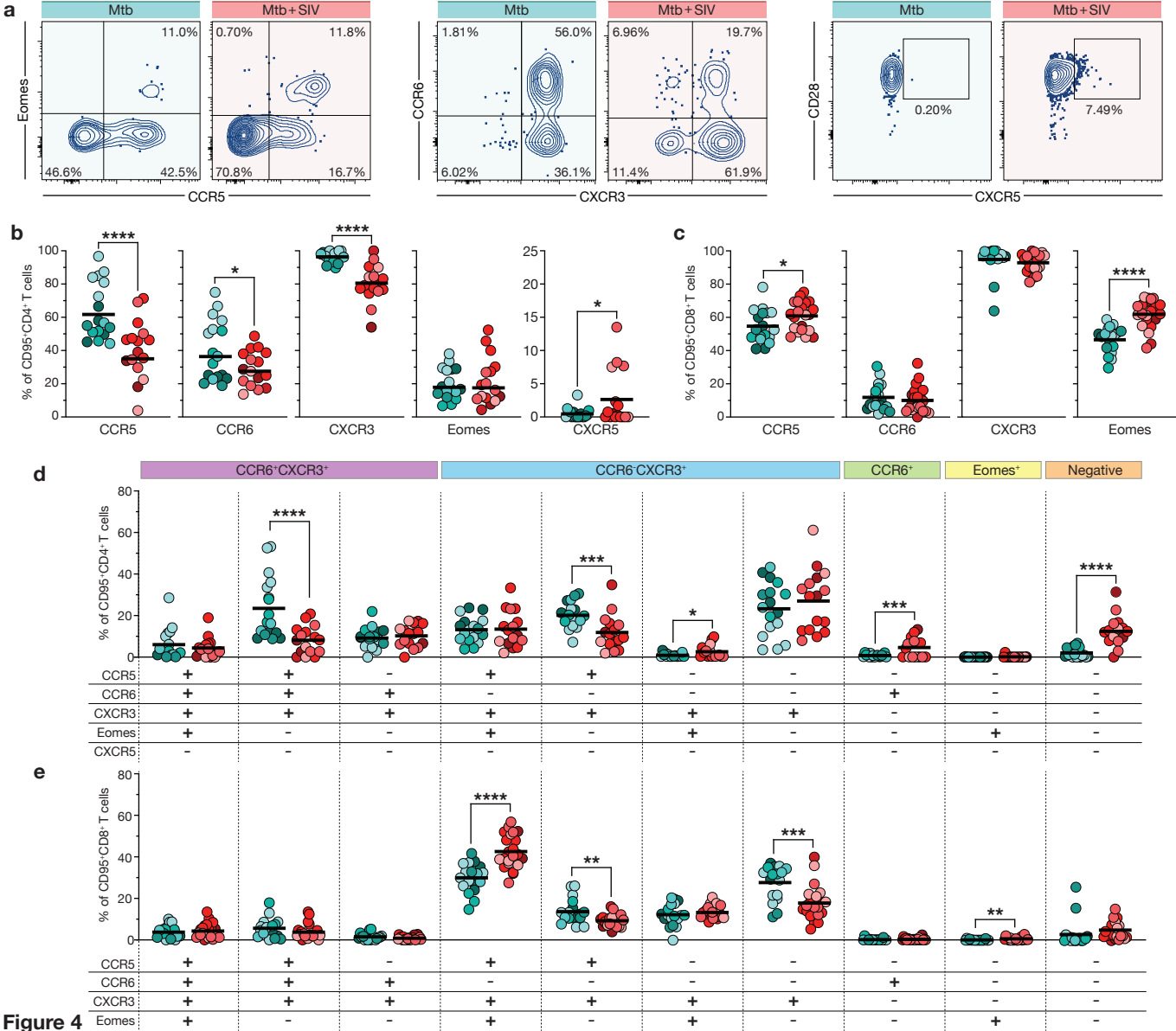687

Figure 1

Figure 2

Figure 3

Figure 4

a CD4 CD20 CD11b

250μm

b
CD4+ Tracks *CD20+ Tracks*

Y-start position
X-start position

Localization
Core
Cuff
GrALT

c
# of tracks per volume (Log_{10}/mm³)

CD4+   CD20+

** (over CD4+)

d *CD4+ tracks*

% localization

Core   *Cuff*   *GrALT*

* (over GrALT)

e *CD4+ tracks*

# of tracks (Log_{10})

Core   *Cuff*   *GrALT*

** (over Core)   * (over Cuff)

f *CD4+ Tracks*

Track Speed Variation (μm per minute)

Mean Track Speed (μm per minute)

SIV- Granuloma
| | 8.25 |
Stopped | 49.7 | 42.0 |
| *Stuttering* |
| *Steady* |

SIV+ Granuloma
| | 11.9 |
Stopped | 78.2 | 9.84 |
| *Stuttering* |
| *Steady* |

g
Stopped

% of tracks

CD4+   CD20+

* (over CD4+)

Steady

% of tracks

CD4+   CD20+

* (over CD4+)

Stuttering

% of tracks

CD4+   CD20+

Figure 5